

Single-Hessian thawed Gaussian approximation: The missing rung on the ladder

Tomislav Begušić,^{a)} Manuel Cordova, and Jiří Vaníček^{b)}

Laboratory of Theoretical Physical Chemistry, Institut des Sciences et Ingénierie Chimiques, Ecole Polytechnique Fédérale de Lausanne (EPFL), CH-1015, Lausanne, Switzerland

(Dated: 15 December 2024)

To alleviate the computational cost associated with on-the-fly *ab initio* semiclassical calculations of molecular spectra, we propose the single-Hessian thawed Gaussian approximation, in which the Hessian of the potential energy at all points along an anharmonic classical trajectory is approximated by a constant value. The spectra obtained with this approximation are compared with the exact quantum spectra of a one-dimensional Morse potential and with the experimental spectra of ammonia and quinquethiophene. In all cases, the single-Hessian version performs almost as well as the much more expensive on-the-fly *ab initio* thawed Gaussian approximation and significantly better than the global harmonic schemes. Remarkably, unlike the thawed Gaussian approximation, the proposed method conserves energy exactly, despite the time dependence of the corresponding effective Hamiltonian.

^{a)}Electronic mail: tomlav.begusic@epfl.ch

^{b)}Electronic mail: jiri.vanicek@epfl.ch

I. INTRODUCTION

Simulation of vibrationally resolved electronic spectra of large polyatomic molecules is a challenge for computational chemistry. The exact calculation is impossible for most but smallest molecular systems due to the exponentially scaling cost of computing the full potential energy surfaces of the electronic states involved in the transition. In the well-known time-independent formalism, the intensities of the individual vibronic transitions are determined by the Franck–Condon factors, i.e., the squares of overlaps between the vibrational eigenstates of the two electronic states, while the frequencies of transitions are given by the differences of the corresponding vibrational eigenvalues. The commonly used method for computing vibronic spectra constructs global harmonic models of the two potential energy surfaces.^{1–3} Then, the vibrational functions, as well as their overlaps, are given analytically. Anharmonic corrections can be included in a perturbative^{4–7} or variational^{8–11} way. For smaller systems it is feasible to apply anharmonic corrections to both eigenstates and eigenvalues, which affects both positions and intensities of vibronic transitions.^{5,10,12} For larger systems, however, this is computationally challenging and the anharmonic corrections are almost exclusively included only through the frequencies, without affecting the Franck–Condon factors.^{7,13,14}

Time-dependent approaches, based on computing the dipole time correlation function,^{15–17} have also been developed at different levels of accuracy, ranging from global harmonic models¹⁸ to exact quantum dynamics methods¹⁹ on anharmonic potential energy surfaces. The time-dependent formalism allows for an on-the-fly implementation, where the potential data are evaluated only when needed, and therefore provides an easier route to including the anharmonicity. We focus our attention on the thawed Gaussian approximation,^{20,21} which, as several other semiclassical^{22–27} and quantum^{28–30} dynamics methods, has been implemented in an on-the-fly fashion and combined with an *ab initio* evaluation of the potential.^{31,32} The method assumes the validity of the Born–Oppenheimer approximation and propagates a Gaussian wavepacket in a locally harmonic potential constructed about the current center of the wavepacket at each time step. This rather simple wavepacket propagation scheme has been proposed by Heller as a first step beyond the global harmonic approximation in the hierarchy of the time-dependent methods. To further reduce the computational cost of the on-the-fly *ab initio* calculations, a Hessian interpolation scheme can be employed, i.e.,

the Hessians are evaluated only every several steps and interpolated in between.³¹

Here, we propose a new approach based on the thawed Gaussian approximation, which still uses a fully anharmonic classical trajectory to guide the Gaussian wavepacket but only a single Hessian to propagate the width. Hence, the single-Hessian approximation further reduces the cost of spectra calculations to that of a single classical trajectory. The method is validated on a one-dimensional Morse potential, as well as on the full-dimensional on-the-fly *ab initio* simulations of the absorption spectrum of ammonia and the emission spectrum of quinquethiophene. It performs better than the global harmonic approaches and in some cases even better than the standard thawed Gaussian approximation. Finally, we demonstrate that, although the effective Hamiltonian associated to the single-Hessian thawed Gaussian approximation is time-dependent, the energy is conserved both analytically and numerically.

II. THEORY

A. Time-dependent approach to vibrationally resolved electronic spectroscopy

Let $|\psi(t)\rangle$ be a wavepacket propagated with a time-independent Hamiltonian H :

$$|\psi(t)\rangle = e^{-i\hat{H}t/\hbar}|\psi_i\rangle, \quad (1)$$

with $|\psi_i\rangle$ representing the initial wavepacket. Within the electric dipole approximation, first-order perturbation theory, and assuming the Condon approximation, vibrationally resolved electronic spectra can be computed from the wavepacket autocorrelation function

$$C(t) = \langle\psi_i|\psi(t)\rangle. \quad (2)$$

The type of spectroscopy is determined by the choice of ψ_i and H . When the initial wavepacket ψ_i is a vibrational eigenstate of the ground electronic state and H the excited-state vibrational Hamiltonian, the rotationally averaged absorption cross-section is evaluated as the Fourier transform^{15,17,33}

$$\sigma_{\text{abs}}(\omega) = \frac{4\pi\omega}{3\hbar c} |\vec{\mu}_{21}|^2 \text{Re} \int_0^\infty C(t) e^{i(\omega + E_{1,i}/\hbar)t} dt, \quad (3)$$

where $E_{1,i}$ is the energy of the vibrational state ψ_i of the ground electronic state 1 and $\vec{\mu}_{21}$ is the transition dipole moment between the ground and excited electronic states evaluated

at the ground-state equilibrium geometry. The emission spectrum, which is measured as the emission rate per unit frequency, is obtained by taking the ψ_i to be the vibrational eigenstate of the excited electronic state and H the ground-state vibrational Hamiltonian:^{33,34}

$$\sigma_{\text{em}}(\omega) = \frac{4\omega^3}{3\pi\hbar c^3} |\vec{\mu}_{21}|^2 \text{Re} \int_0^\infty C(t)^* e^{i(\omega - E_{2,i}/\hbar)t} dt, \quad (4)$$

with $E_{2,i}$ the energy of the vibrational state ψ_i of the excited electronic state 2. The spectra defined in Eqs. (3) and (4) are positive at all frequencies—this can be shown by inserting a resolution of identity in the expression for the autocorrelation function to derive the time-independent expression; e.g., for the absorption spectrum, one obtains¹⁷

$$\sigma_{\text{abs}}(\omega) = \frac{4\pi^2\omega}{3\hbar c} |\vec{\mu}_{21}|^2 \sum_n |\langle n|\psi_i\rangle|^2 \delta(\omega - \frac{E_{2,n} - E_{1,i}}{\hbar}), \quad (5)$$

where $|n\rangle$ are the eigenstates of the excited-state vibrational Hamiltonian with energies $E_{2,n}$. The equivalence of the Eqs. (3) and (5) is valid for any time-independent Hamiltonian. However, if one attempts to approximate the true time-independent Hamiltonian by an effective time-dependent one, for example, through the local harmonic or cubic approximations,³² negative spectral features may arise.

B. Thawed Gaussian approximation

The evaluation of the autocorrelation function (2) requires the propagation of the vibrational wavepacket; among many quantum and semiclassical methods, one of the simplest is the thawed Gaussian approximation. A thawed Gaussian wavepacket is described by its time-dependent position q_t , momentum p_t , complex symmetric matrix A_t , and a complex number γ_t :

$$\psi(q, t) = N_0 \exp \left\{ -(q - q_t)^T \cdot A_t \cdot (q - q_t) + \frac{i}{\hbar} [p_t^T \cdot (q - q_t) + \gamma_t] \right\}, \quad (6)$$

where N_0 is the normalization constant. The classical parameters, q_t and p_t , are the expectation values of the position and momentum; the real part of the matrix A_t is related to the width of the wavepacket, while its imaginary part introduces a spatial chirp; the real part of the number γ_t is a time-dependent phase factor and the imaginary part of γ_t ensures the normalization of the wavepacket at all times. The Gaussian form of the wavepacket is exactly preserved in a harmonic potential, even a time-dependent one. In the thawed

Gaussian approximation the wavepacket (6) is propagated with an effective Hamiltonian $\hat{H}_{\text{eff}}(t) = \hat{T} + \hat{V}_{\text{LHA}}(t)$ given by the sum of the kinetic energy T and the time-dependent local harmonic approximation V_{LHA} of the true potential V about q_t :

$$V_{\text{LHA}}(q, t) = V(q_t) + \text{grad}_q V|_{q_t}^T \cdot (q - q_t) + \frac{1}{2}(q - q_t)^T \cdot \text{Hess}_q V|_{q_t} \cdot (q - q_t), \quad (7)$$

with $\text{grad}_q V|_{q_t}$ representing the gradient and $\text{Hess}_q V|_{q_t}$ the Hessian of the potential V evaluated at the center of the wavepacket q_t . Inserting the Gaussian ansatz and the effective potential into the time-dependent Schrödinger equation results in the following equations of motion for the wavepacket parameters:²⁰

$$\dot{q}_t = m^{-1} \cdot p_t, \quad (8)$$

$$\dot{p}_t = -\text{grad}_q V|_{q_t}, \quad (9)$$

$$\dot{A}_t = -2i\hbar A_t \cdot m^{-1} \cdot A_t + \frac{i}{2\hbar} \text{Hess}_q V|_{q_t}, \quad (10)$$

$$\dot{\gamma}_t = L_t - \hbar^2 \text{Tr} \left(m^{-1} \cdot A_t \right), \quad (11)$$

where m is the mass matrix and L_t the Lagrangian.

If the wavepacket stays localized during the dynamics, the effective locally harmonic potential is a valid approximation of the exact potential. In such cases, the thawed Gaussian approximation is expected to yield a rather accurate wavepacket propagation. The approximation accounts partially for the anharmonicity of the potential by propagating the wavepacket's center (q_t, p_t) classically with the true potential $V(q)$ [Eqs. (8)–(9)] and by accounting for the changes in the Hessian of the potential, which affect the semiclassical parameters A_t and γ_t . Another advantage of the thawed Gaussian propagation is its efficiency: it requires the propagation of four time-dependent parameters, which depend only on the local potential information.

Yet, there are several disadvantages of such a simple wavepacket propagation scheme. First, the Gaussian ansatz cannot describe wavepacket splitting, tunneling, or nonadiabatic effects. In systems with significant anharmonicity, where the exact wavepacket splits and delocalizes quickly, the thawed Gaussian wavepacket behaves unphysically. Second, because the effective potential of Eq. (7) is, in general (i.e., for potentials beyond quadratic), time-

dependent, the thawed Gaussian approximation does not conserve energy:^{32,35}

$$\frac{dE}{dt} = \frac{d}{dt} \langle \psi(t) | \hat{H}_{\text{eff}}(t) | \psi(t) \rangle \quad (12)$$

$$= \langle \psi(t) | \frac{d}{dt} \hat{H}_{\text{eff}}(t) | \psi(t) \rangle \quad (13)$$

$$= \langle \psi(t) | \frac{d}{dt} \hat{V}_{\text{LHA}}(t) | \psi(t) \rangle \quad (14)$$

$$= \frac{1}{2} \langle \psi(t) | (\hat{q} - q_t)^T \cdot B_t \cdot (\hat{q} - q_t) | \psi(t) \rangle \quad (15)$$

$$= \frac{1}{2} \text{Tr}(B_t \cdot \Sigma_t^2), \quad (16)$$

where $B_t := p_t^T \cdot m^{-1} \cdot V'''|_{q_t}$, V''' is a rank-3 tensor of third derivatives of the potential with respect to position, and

$$\begin{aligned} \Sigma_t^2 &:= \langle \psi(t) | (\hat{q} - q_t) \otimes (\hat{q} - q_t)^T | \psi(t) \rangle \\ &= \int dq |\psi(q, t)|^2 (q - q_t) \otimes (q - q_t)^T \\ &= (4 \text{Re } A_t)^{-1} \end{aligned}$$

is the position covariance matrix. Equation (13) follows from the fact that the thawed Gaussian wavepacket solves exactly the time-dependent Schrödinger equation with H_{eff} , while Eq. (14) relies on the time independence of the kinetic energy operator. To derive Eq. (15), we used the chain rule

$$\frac{d}{dt} = p_t^T \cdot m^{-1} \cdot \frac{d}{dq_t} \quad (17)$$

for the differentiation of the energy, gradient, and Hessian evaluated at position q_t . As noted already in Section II A, the time dependence of the effective Hamiltonian also leads to unphysical negative intensities in the spectra.

C. Hessian interpolation

To reduce the cost of *ab initio* Hessian calculations, the on-the-fly *ab initio* thawed Gaussian approximation is readily combined with an interpolation scheme, where the Hessians are computed only every few steps and the intermediate Hessians are obtained from a second-order polynomial interpolation. Typically, the Hessians need to be computed only every 4 to 8 time steps.^{31,36} Since the Hessians are not needed for the propagation of the classical

trajectory, additional speed-up is achieved through parallel computation of the Hessians after the full trajectory is known. Note that other Hessian approximations, such as the Hessian update schemes^{37–39} and Gaussian process regression^{40,41} have been developed in the context of *ab initio* simulations. The considerable cost of multiple Hessian evaluations has also inspired various semiclassical approximations,⁴² including the prefactor-free²² and “poor person’s”⁴³ variations of the Herman–Kluk propagator.

D. Global harmonic approximation

In computational chemistry, most of the calculations of vibrationally resolved electronic spectra are based on the global harmonic models, where a harmonic approximation

$$V_{\text{HA}}(q) = V_{eq} + \frac{1}{2}(q - q_{eq})^T \cdot k \cdot (q - q_{eq}) \quad (18)$$

to the true potential energy surface is used. In Eq. (18), V_{eq} is the potential energy and q_{eq} the position of the minimum of the harmonic potential with a force constant matrix k . In practice, the global harmonic model is constructed from *ab initio* data evaluated at only one molecular geometry, which makes such calculations computationally feasible even for rather large systems. The thawed Gaussian wavepacket (6) is exact for the harmonic potential (18) and can be propagated analytically. Furthermore, because the potential is time-independent, the energy is exactly conserved and the corresponding spectra do not suffer from unphysical negative intensities. However, the method neglects the anharmonicity effects completely and, as a consequence, is less accurate than the thawed Gaussian approximation.

E. Single-Hessian thawed Gaussian approximation

Let us now consider using a single Hessian in the local harmonic approximation of Eq. (7), e.g., by choosing a reference $\text{Hess}_q V_{\text{ref}}$ and approximating the potential at each point in time as

$$V_{\text{SH}}(q, t) = V(q_t) + \text{grad}_q V|_{q_t}^T \cdot (q - q_t) + \frac{1}{2}(q - q_t)^T \cdot \text{Hess}_q V_{\text{ref}} \cdot (q - q_t). \quad (19)$$

Regarding the computational effort, the single-Hessian thawed Gaussian approximation, which propagates a Gaussian wavepacket [Eq. (6)] in the effective potential of Eq. (19), is even more efficient than the thawed Gaussian approximation; the single-Hessian analogue

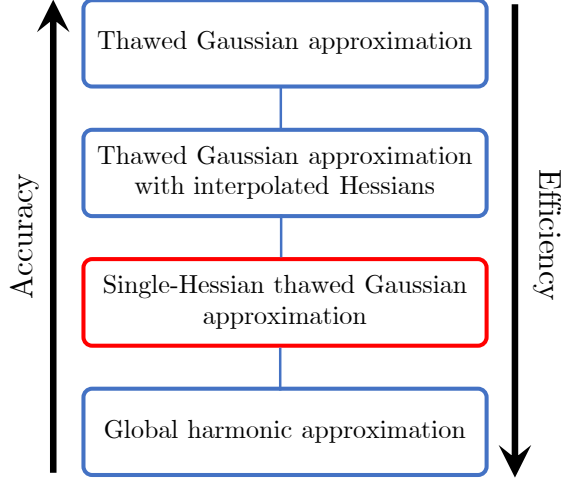


FIG. 1. Hierarchy of several semiclassical time-dependent wavepacket methods for simulating vibrationally resolved electronic spectra.

requires only one Hessian to be evaluated for the whole propagation, i.e., its cost is almost the same as running a single classical trajectory. Because the effective potential (19) is Hermitian, the single-Hessian method conserves the norm of the wavefunction. As for the accuracy, the approximation of the potential given in Eq. (19) still includes the anharmonicity partially through the first two terms and is more accurate than the global harmonic approximation, but is clearly worse than the local harmonic approximation of Eq. (7) (see Fig. 1); however, the single-Hessian approach also results in several improvements related to spectra calculations.

First, there is an important difference in the propagation of the time-dependent parameters of the wavepacket—the dynamics of the matrix A_t is now determined exclusively by the reference Hessian and is decoupled from the classical dynamics of q_t and p_t . Therefore, the wavepacket does not spread or contract unphysically in an attempt to describe the wavepacket splitting, but rather stays compact at all times, as if propagated in a globally harmonic potential. We show in several numerical examples that this feature is preferred in more anharmonic potentials.

Second, the single-Hessian thawed Gaussian approximation conserves energy exactly:

$$\frac{dE}{dt} = \langle \psi(t) | \frac{d}{dt} \hat{V}_{\text{SH}}(t) | \psi(t) \rangle \quad (20)$$

$$= \langle \psi(t) | b_t^T \cdot (\hat{q} - q_t) | \psi(t) \rangle \quad (21)$$

$$= b_t^T \cdot \langle \psi(t) | \hat{q} - q_t | \psi(t) \rangle \quad (22)$$

$$= 0, \quad (23)$$

where $b_t^T := p_t^T \cdot m^{-1} \cdot (\text{Hess}_q V|_{q_t} - \text{Hess}_q V_{\text{ref}})$. Above, we used the time independence of the kinetic energy operator in Eq. (20) and the chain rule (17) to go from Eq. (20) to (21). The final result (23) follows from Eq. (22) because q_t is the expectation value of the position operator \hat{q} in the state $\psi(t)$. Despite the energy conservation, the effective Hamiltonian determined by the effective potential of Eq. (19) is still time-dependent—the energy is conserved only because the Hamiltonian is nonlinear (i.e., it depends on the state ψ) and its change applied to ψ happens to be “orthogonal” to the state ψ [Eqs. (20)–(23)]. Therefore, the conservation of energy does not guarantee non-negative intensities in the spectrum. Yet, the hope is that the negative spectral features in the single-Hessian approach will be less pronounced than in the standard thawed Gaussian approximation.

F. Reference Hessians

Both global harmonic models and single-Hessian thawed Gaussian approximation depend on the choice of the reference Hessian. Two well-known special choices are the adiabatic Hessian, evaluated at the minimum of the final electronic surface, and the vertical Hessian, evaluated at the initial geometry, i.e., the minimum of the initial electronic surface.^{13,44} When combined with the global harmonic approach, we refer to these as the *adiabatic harmonic* and *vertical harmonic* methods.^{31,45,46} These global harmonic models are sometimes referred to as the adiabatic and vertical Hessian,^{13,18,44} here, we use these names exclusively for the Hessians to avoid the confusion between the single-Hessian thawed Gaussian propagation and global harmonic methods. The combinations of the single-Hessian approach with the different reference Hessians will be referred to as the *adiabatic single-Hessian* and *vertical single-Hessian* methods.

Finally, one can avoid computing an additional Hessian by setting the reference as the initial-state Hessian, which is commonly needed for constructing the initial wavepacket. In

the context of the global harmonic methods, there are two natural possibilities of constructing a final-state harmonic potential using the initial-state Hessian: one can either compute the potential energy and gradient of the final-state potential energy surface at the initial geometry, which results in the *vertical gradient* model, or optimize the geometry in the final electronic state, which corresponds to the *adiabatic shift* model.^{13,44,47} Both the vertical gradient and adiabatic shift models are examples of displaced harmonic systems, and thus ignore mode distortion and mixing (the Duschinsky effect) between the two electronic states. In the results section, we discuss only the adiabatic shift model and, for consistency with the other methods discussed in this work, refer to it as the *initial harmonic* model. Finally, the *initial single-Hessian* approach, which uses the initial Hessian for the single-Hessian thawed Gaussian propagation, is equivalent to the propagation of a “frozen Gaussian”⁴⁸ with a constant matrix $A_t = A_0$ and

$$\gamma_t = S_{\text{cl},t} - \hbar^2 \text{Tr} (m^{-1} \cdot A_0) t \quad (24)$$

$$= S_{\text{cl},t} - t \sum_{i=1}^F \frac{1}{2} \hbar \omega_i, \quad (25)$$

where $S_{\text{cl},t} := \int L_t dt$ is the classical action, F is the number of vibrational degrees of freedom, and ω_i are the frequencies corresponding to the initial Hessian.

III. COMPUTATIONAL DETAILS

A. Morse potential

To investigate the single-Hessian thawed Gaussian approximation in systems of varying anharmonicity, we constructed a series of Morse potentials:

$$V(q) = V_{\text{eq}} + D[1 - e^{-a(q-q_{\text{eq}})}]^2, \quad (26)$$

with different values of the dissociation energy D and anharmonicity parameter a . In Eq. (26) V_{eq} is the potential at the equilibrium position q_{eq} . We chose to work in atomic units ($\hbar = 1$) and mass-scaled coordinates. The Morse parameters were $V_{\text{eq}} = 0.1$ and $q_{\text{eq}} = \sqrt{2/\omega_{\text{eq}}}$. We also fixed the global harmonic potential fitted to the Morse potentials at the equilibrium position q_{eq} ; its frequency,

$$\omega_{\text{eq}} = \sqrt{\text{Hess}_q V|_{q_{\text{eq}}}} = \sqrt{2Da^2}, \quad (27)$$

was set to 0.0041 a.u. = 900 cm⁻¹. The anharmonicity of the potential was controlled through the dimensionless anharmonicity constant

$$\chi = \frac{\omega_{\text{eq}}}{4D}. \quad (28)$$

Then, the d and a parameters were uniquely defined as

$$D = \frac{\omega_{\text{eq}}}{4\chi}, \quad (29)$$

$$a = \sqrt{2\omega_{\text{eq}}\chi}. \quad (30)$$

The initial wavepacket was a real Gaussian with zero position and momentum, and with the width corresponding to the ground vibrational state of a one-dimensional harmonic oscillator of frequency 0.00456 a.u. = 1000 cm⁻¹. The transition dipole moment was set to 1. The wavepacket was propagated on the Morse potential energy surfaces of different degrees of anharmonicity for 4000 steps of 8 a.u. \approx 0.194 fs. Spectra evaluated with the thawed-Gaussian, global harmonic, and single-Hessian approaches discussed in Section II F were compared with the exact quantum dynamics calculations, obtained with the second-order split-operator method. The position grid for the exact quantum dynamics consisted of 16384 points between -200 and 200 atomic units. To avoid artifacts of the finite-time calculation, all correlation functions were multiplied by a Gaussian damping function corresponding to the Gaussian broadening with half-width at half-maximum of 115 cm⁻¹. Then, the spectra were computed according to Eq. (3) and scaled according to the maximum intensity.

B. On-the-fly *ab initio* calculations

The on-the-fly *ab initio* implementation of the thawed Gaussian approximation has been detailed in Refs. 31, 32, 45, and 46. Briefly, the method evaluates the required potential information along the trajectory from an *ab initio* electronic structure program. Our in-house code performs the dynamics, transformation between Cartesian and normal-mode coordinates, and interpolation of the Hessians if they are not computed at each step (see Refs. 31 and 45).

For ammonia, the *ab initio* calculations were performed using the complete active-space second-order perturbation theory, CASPT2(8/8), in combination with the aug-cc-pVTZ basis set, as implemented in the Molpro2012.1 package.^{49,50} For the quinquethiophene, the

ground-state potential data were evaluated using the density functional theory, while the time-dependent density functional theory was used for geometry optimization and Hessian calculations in the first excited electronic state; the functional was B3LYP and the basis set 6-31+G(d,p), as implemented in Gaussian09.⁵¹ All trajectories were propagated using a time step of 8 a.u. for 1000 steps in ammonia and for 997 steps in quinquethiophene. As for the Hessian calculations, in ammonia we computed the Hessian at each step, whereas in quinquethiophene we applied the interpolation scheme, with the Hessian evaluated only every four steps of the classical trajectory and interpolated in between; this interpolation step was previously validated in Ref. 31. Before computing the spectra, the correlation functions were multiplied by a Gaussian damping function corresponding to the Gaussian broadening with half-width at half-maximum of 200 cm⁻¹. Further computational details can be found in Ref. 32 for the ammonia absorption spectrum and in Ref. 31 for the quinquethiophene spontaneous emission spectrum.

IV. RESULTS AND DISCUSSION

A. Morse potential

Figure 2 compares the exact spectra of two Morse potentials of different degrees of anharmonicity with those evaluated using the standard thawed Gaussian approximation, its adiabatic single-Hessian version, and the adiabatic harmonic method. In the weakly anharmonic potential (Fig. 2, left), all methods perform well, with only the global harmonic spectrum deviating slightly from the exact solution. In contrast, in the more anharmonic Morse potential, the adiabatic harmonic model recovers only the first few peaks. Interestingly, the single-Hessian version seems to be more accurate than the standard thawed Gaussian approximation—although the corresponding peak positions overlap, the intensities are described better in the single-Hessian approximation.

To quantify the accuracy of the approaches discussed in Section II F, we introduce the spectral contrast angle θ between a reference (σ_{ref}) and approximate (σ) spectra, conveniently defined through its cosine

$$\cos \theta = \frac{\sigma_{\text{ref}} \cdot \sigma}{\|\sigma_{\text{ref}}\| \|\sigma\|}, \quad (31)$$

with the inner product $\sigma_1 \cdot \sigma_2 = \int d\omega \sigma_1(\omega) \sigma_2(\omega)$ of two spectra and norm of a spectrum

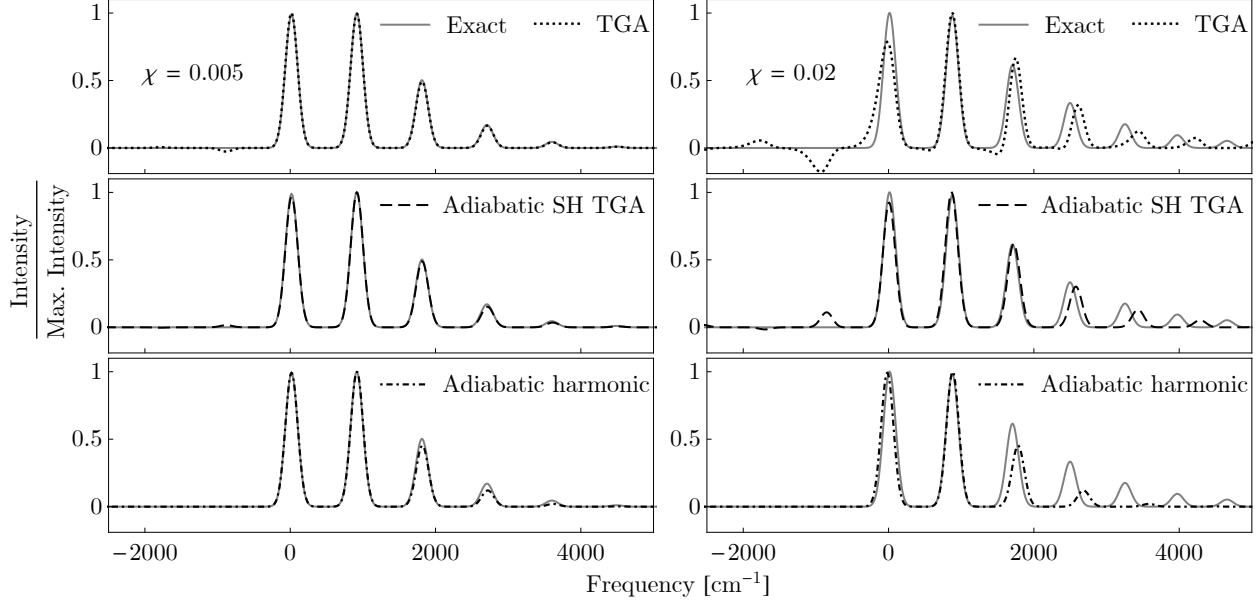


FIG. 2. Spectra of two Morse potentials with different anharmonicity constants χ evaluated using the exact quantum dynamics, thawed Gaussian approximation (TGA, top), adiabatic single-Hessian thawed Gaussian approximation (SH TGA, middle), and adiabatic harmonic model (bottom). Left: $\chi = 0.005$. Right: $\chi = 0.02$. All spectra were shifted to give the best overlap with the exact calculation and the zero frequency was set to the 0–0 transition, i.e., the first peak of the progression.

$\|\sigma\| = \sqrt{\sigma \cdot \sigma}$. Spectra evaluated with the exact quantum dynamics are used as reference. In *ab initio* calculations, the errors in the absolute frequency shift of the spectrum originate mostly from the limited accuracy of the electronic structure methods. Therefore, even in the Morse potential, we first maximize the overlap with the reference by shifting the computed spectra in frequency and then evaluate the spectral contrast angle. The maximum overlap is found by scanning through all possible shifts, with the increment determined by the numerical resolution of the spectrum.

As shown in Fig. 3, the accuracies of all presented methods decrease with increasing anharmonicity of the potential. However, the methods based on the thawed Gaussian approximation clearly perform better than the global harmonic approaches. Moreover, the single-Hessian results are nearly the same for all three choices of the Hessian, which is not the case for the global harmonic approximations. The errors in the spectra of more anharmonic potentials (see Fig. 2) correspond mainly to the incorrect peak spacings, which

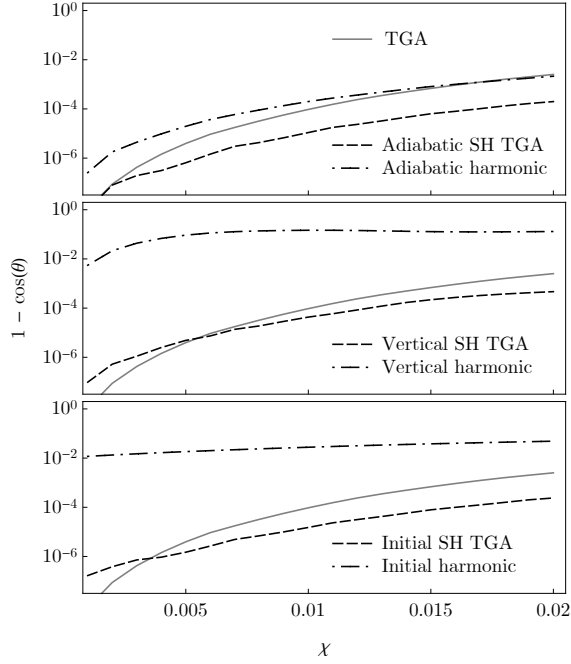


FIG. 3. Spectral contrast angles for Morse potentials with different anharmonicity constants χ . The angles [Eq. 31] compare approximate spectra evaluated using the thawed Gaussian approximation (TGA), its single-Hessian (SH) versions, and global harmonic methods with the exact spectrum. The single-Hessian and global harmonic results are presented for three different choices of the reference Hessian: adiabatic, vertical, and initial.

are almost exclusively determined by the classical trajectory guiding the thawed Gaussian wavepacket—therefore, in the single-Hessian thawed Gaussian approximation the choice of the Hessian affects the result only weakly.

Negative intensities in the spectra computed with the thawed Gaussian approximation further increase the errors measured by the spectral contrast angle. Such features are nearly eliminated in the single-Hessian version of the thawed Gaussian approximation, which conserves energy exactly (see Fig. 4); however, negative intensities still arise even in the single-Hessian method due to the time-dependence of the effective single-Hessian potential (19).

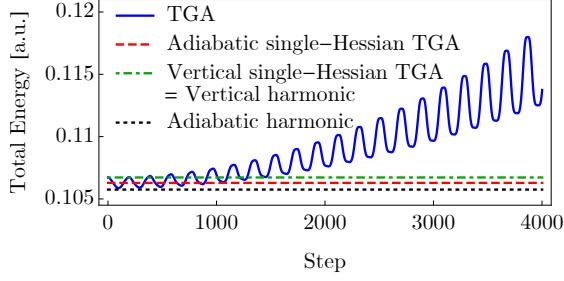


FIG. 4. Total energy of the wavepackets propagated in a Morse potential ($\chi = 0.005$, see Sec. III A) using the thawed Gaussian approximation (TGA), two single-Hessian approaches, and two harmonic models. For the initial single-Hessian thawed Gaussian approximation (not shown for clarity), the energy is a horizontal line between those corresponding to the adiabatic and vertical single-Hessian approaches.

B. Absorption spectrum of ammonia

Ammonia is a prototypical example of a floppy system, i.e., a system exhibiting large-amplitude motion. Electronic excitation to the first excited state is accompanied by a significant displacement of the umbrella inversion mode, allowing the generated wavepacket to visit anharmonic regions of the excited-state potential energy surface. Due to the small size of the system, rich nuclear dynamics, and available experimental data, the absorption, emission, and photoelectron spectra of ammonia have served as benchmarks for different methods built specifically to treat the anharmonicity effects.^{52–55} In particular, the on-the-fly *ab initio* thawed Gaussian approximation showed significant improvement over the global harmonic models.³²

Figure 5 compares the global harmonic and single-Hessian approaches with the on-the-fly *ab initio* thawed Gaussian approximation³² and with the experimental absorption spectrum of ammonia.⁵⁶ All single-Hessian methods recover both the peak positions and intensities of the standard thawed Gaussian approximation. In contrast, all global harmonic models yield different and rather inaccurate spectra. Most interesting are the adiabatic single-Hessian thawed Gaussian approximation and adiabatic global harmonic model: although both methods use only one (adiabatic) Hessian, the former performs better than any other presented method, including the standard thawed Gaussian approximation, whereas the latter performs the worst. These results indicate that the single-Hessian thawed Gaussian

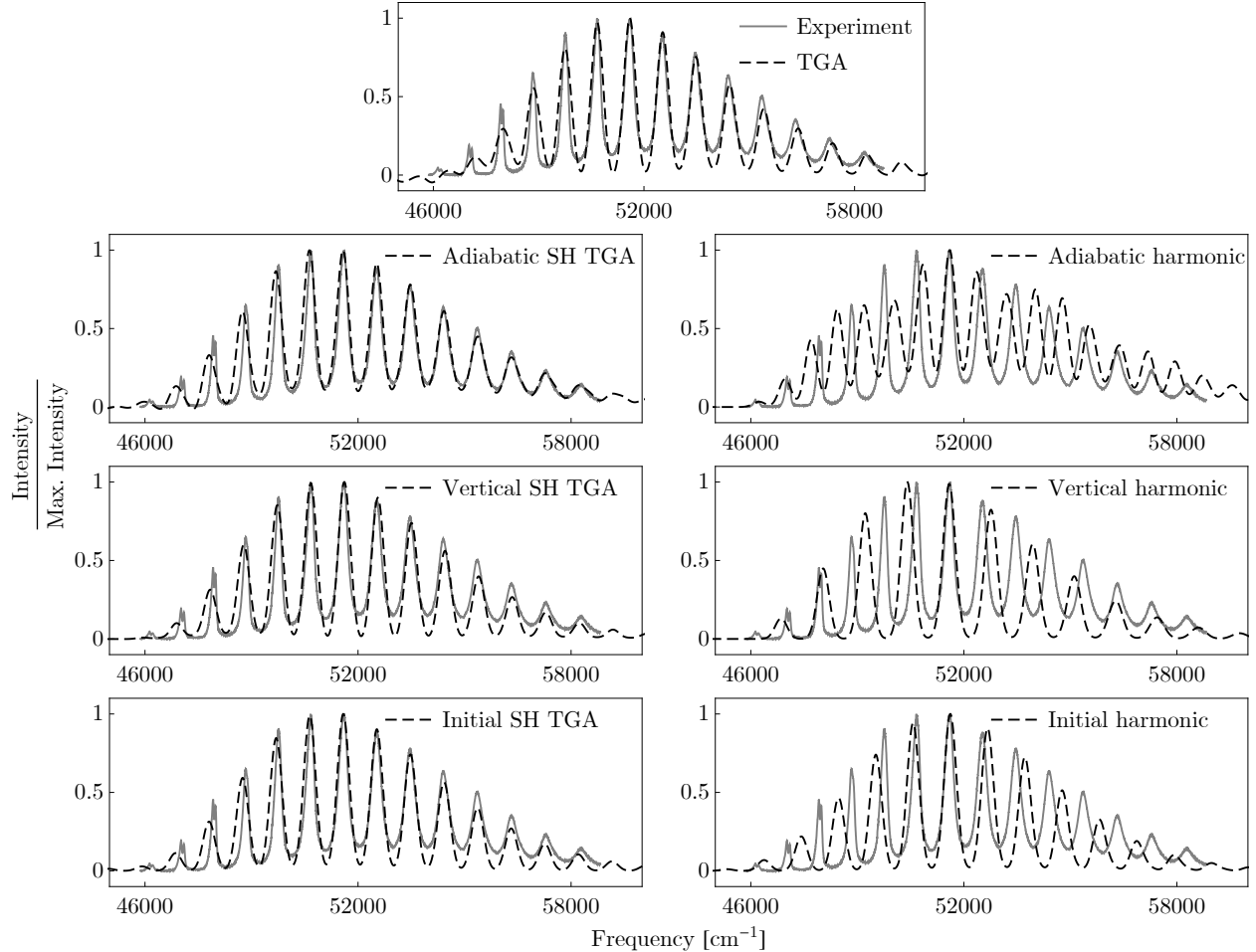


FIG. 5. Experimental absorption spectra of ammonia measured in gas phase at 175 K⁵⁶ compared with those evaluated using the on-the-fly *ab initio* thawed Gaussian approximation (TGA), its single-Hessian (SH) version, and global harmonic models. The single-Hessian and global harmonic results are presented for three different choices of the reference Hessian: adiabatic, vertical, and initial. Computed spectra were scaled and shifted according to the highest peak of the experiment.

approximation cannot be discarded in advance based on the performance of global harmonic models; in fact, its accuracy is much closer to that of the thawed Gaussian approximation. Indeed, even the initial (ground-state) single Hessian approach reproduces almost perfectly the result of the standard on-the-fly *ab initio* thawed Gaussian approximation.

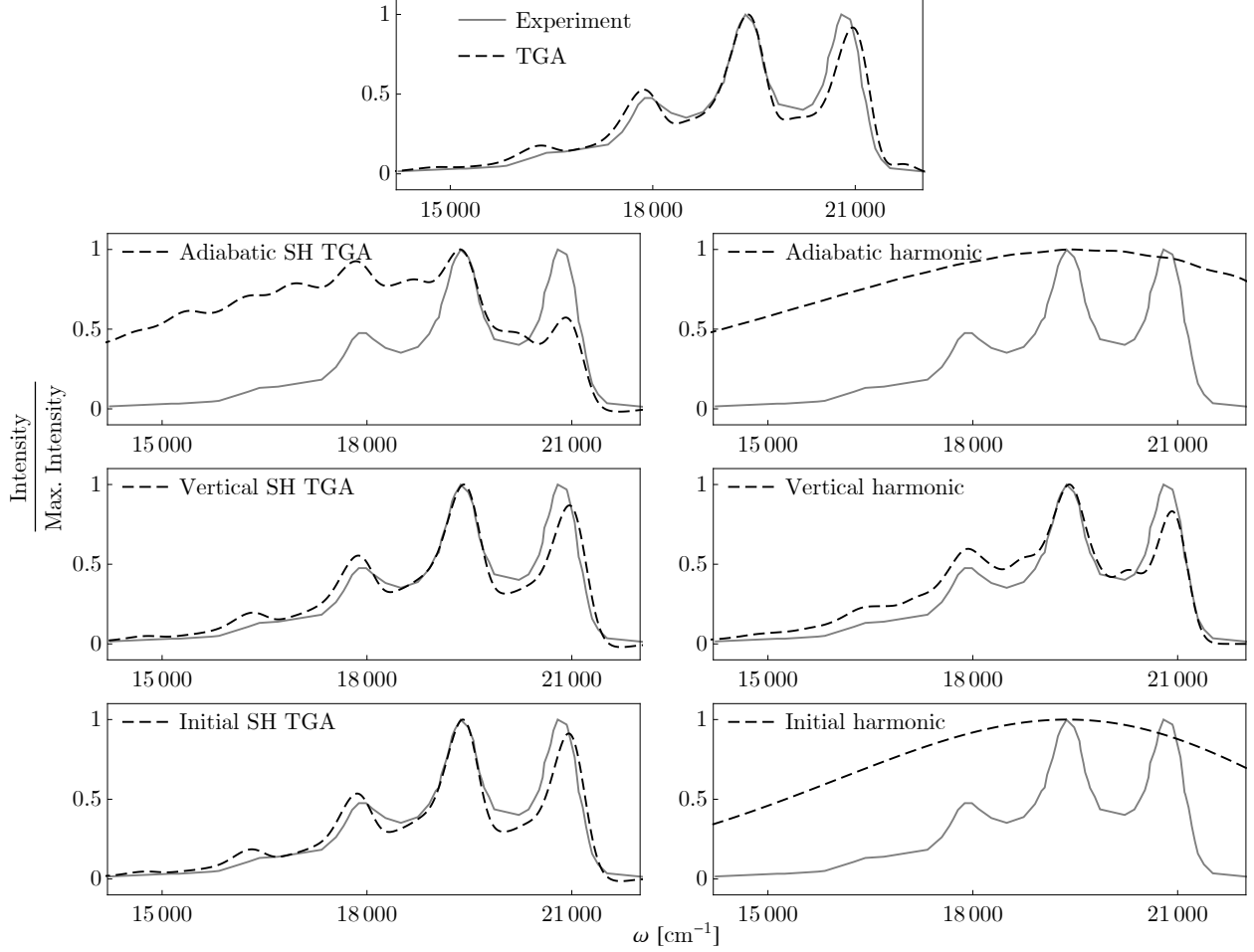


FIG. 6. Analogous to Fig. 5, but for the emission spectrum of quinquethiophene. The experiment was measured in ethanol glass at 77 K.⁵⁷

C. Emission spectrum of quinquethiophene

Due to their potential in molecular electronics, polythiophenes and their derivatives have been studied extensively. Oligothiophenes have also served as a model system for studying the dependence of optical properties on the system size. They present a challenge for computing vibrationally resolved electronic spectra due to the torsional degrees of freedom, which cannot be treated with global harmonic models. Wehrle et al. showed that the on-the-fly *ab initio* thawed Gaussian approximation performs well despite the double-well character of the potential along the torsional modes connecting the planar and twisted structures.

In Fig. 6, we compare the experimental⁵⁷ emission spectrum of quinquethiophene, an oligomer composed of five thiophene units, and corresponding spectra computed with vari-

ous approximations discussed in Section II. The single-Hessian approaches using the initial (excited-state) and vertical Hessians produce almost the same spectra as the standard thawed Gaussian approximation³¹ (shown in Fig. 6, top). However, this is not the case for the adiabatic single-Hessian method, which yields a broad spectrum due to the incorrect description of the torsional degrees of freedom. As discussed in Ref.³¹, the initial wavepacket is placed at the top of a potential barrier along the torsional modes, which results in a constant but slow wavepacket spreading. The adiabatic Hessian has all frequencies positive and is therefore qualitatively inappropriate. Interestingly, the initial single-Hessian approach, which propagates a frozen Gaussian, results in a rather accurate spectrum, implying that the errors of using the adiabatic Hessian arise due to the incorrect width of the Gaussian wavepacket.

In contrast, the failure of the adiabatic global harmonic model (Fig. 6, top right) is not related to the Hessian, but rather to the large displacement of the ground-state potential minimum from the initial geometry. The computed emission spectrum is nearly featureless because the wavepacket quickly drifts away from the initial planar geometry and does not return during the short dynamics considered for spectra simulations. This explanation is supported by the equally featureless spectrum of the adiabatic shift model, i.e., the initial harmonic model (see Fig. 6, bottom right), which has the same displacement of the adiabatic global harmonic model but uses the initial (excited-state) Hessian.

V. CONCLUSION

In conclusion, we have presented and validated an efficient method for evaluating vibrationally resolved electronic spectra of polyatomic molecules. The proposed single-Hessian thawed Gaussian approximation, whose computational cost lies between those of the global harmonic and thawed Gaussian approximations, performs surprisingly well, in some cases even better than the more computationally demanding thawed Gaussian approximation. Moreover, unlike the standard thawed Gaussian approximation, the single-Hessian approach conserves total energy exactly. We have shown that despite the conservation of energy, the computed spectra may still contain negative intensities due to the time dependence of the effective Hamiltonian. Yet, the negative spectral features are significantly smaller compared with the standard thawed Gaussian approximation. In contrast to the spectra evaluated using the global harmonic approaches, those computed with the single-Hessian

thawed Gaussian approximation depend only weakly on the reference Hessian. Therefore, the single-Hessian approach offers a considerable and systematic improvement over the commonly used global harmonic models at the cost of a single *ab initio* classical trajectory.

ACKNOWLEDGMENTS

The authors acknowledge the financial support from the European Research Council (ERC) under the European Union’s Horizon 2020 research and innovation programme (grant agreement No. 683069 – MOLEQULE) and from the EPFL.

REFERENCES

- ¹F. Santoro, R. Improta, A. Lami, J. Bloino, and V. Barone, J. Chem. Phys. **126** (2007), 10.1063/1.2437197.
- ²F. Santoro, A. Lami, R. Improta, J. Bloino, and V. Barone, J. Chem. Phys. **128** (2008), 10.1063/1.2929846.
- ³V. Barone, J. Bloino, M. Biczysko, and F. Santoro, J. Chem. Theory Comput. **5**, 540 (2009).
- ⁴S. Bonness, B. Kirtman, M. Huix, A. J. Sanchez, and J. M. Luis, J. Chem. Phys. **125** (2006), 10.1063/1.2210479.
- ⁵J. M. Luis, D. M. Bishop, and B. Kirtman, J. Chem. Phys. **120**, 813 (2004).
- ⁶L. Yang, C. Zhu, J. Yu, and S. H. Lin, Chem. Phys. **400**, 126 (2012).
- ⁷F. Egidi, D. B. Williams-Young, A. Baiardi, J. Bloino, G. Scalmani, M. J. Frisch, X. Li, and V. Barone, J. Chem. Theory Comput. **13**, 2789 (2017).
- ⁸J. M. Luis, B. Kirtman, and O. Christiansen, J. Chem. Phys. **125** (2006), 10.1063/1.2360944.
- ⁹J. M. Bowman, T. Carrington, and H. D. Meyer, Mol. Phys. **106**, 2145 (2008).
- ¹⁰L. Koziol, V. A. Mozhayskiy, B. J. Braams, J. M. Bowman, and A. I. Krylov, J. Phys. Chem. A **113**, 7802 (2009).
- ¹¹P. Meier and G. Rauhut, Mol. Phys. **113**, 3859 (2015).
- ¹²D. K. W. Mok, E. P. F. Lee, F.-T. Chau, D. Wang, and J. M. Dyke, J. Chem. Phys. **113**, 5791 (2000).

- ¹³F. Egidi, J. Bloino, C. Cappelli, and V. Barone, *J. Chem. Theory Comput.* **10**, 346 (2014).
- ¹⁴M. Biczysko, J. Krupa, and M. Wierzejewska, *Faraday Discussions* **212**, 421 (2018).
- ¹⁵E. J. Heller, *Acc. Chem. Res.* **14**, 368 (1981).
- ¹⁶S. Mukamel, *Principles of nonlinear optical spectroscopy*, 1st ed. (Oxford University Press, New York, 1999).
- ¹⁷D. J. Tannor, *Introduction to Quantum Mechanics: A Time-Dependent Perspective* (University Science Books, Sausalito, 2007).
- ¹⁸A. Baiardi, J. Bloino, and V. Barone, *J. Chem. Theory Comput.* **9**, 4097 (2013).
- ¹⁹H.-D. Meyer, F. Gatti, and G. A. Worth, *Multidimensional Quantum Dynamics: MCTDH Theory and Applications* (WILEY-VCH, 2009).
- ²⁰E. J. Heller, *J. Chem. Phys.* **62**, 1544 (1975).
- ²¹F. Grossmann, *J. Chem. Phys.* **125**, 014111 (2006).
- ²²J. Tatchen and E. Pollak, *J. Chem. Phys.* **130**, 041103 (2009).
- ²³M. Ceotto, S. Atahan, S. Shim, G. F. Tantardini, and A. Aspuru-Guzik, *Phys. Chem. Chem. Phys.* **11**, 3861 (2009).
- ²⁴M. Ceotto, S. Atahan, G. F. Tantardini, and A. Aspuru-Guzik, *J. Chem. Phys.* **130**, 234113 (2009).
- ²⁵S. Y. Y. Wong, D. M. Benoit, M. Lewerenz, A. Brown, and P.-N. Roy, *J. Chem. Phys.* **134**, 094110 (2011).
- ²⁶F. Gabas, R. Conte, and M. Ceotto, *J. Chem. Theory Comput.* **13**, 2378 (2017).
- ²⁷F. Gabas, G. Di Liberto, R. Conte, and M. Ceotto, *Chem. Sci.* **9**, 7894 (2018).
- ²⁸M. Ben-Nun, J. Quenneville, and T. J. Martínez, *J. Phys. Chem. A* **104**, 5161 (2000).
- ²⁹K. Saita and D. V. Shalashilin, *J. Chem. Phys.* **137**, 22A506 (2012).
- ³⁰G. Richings, I. Polyak, K. Spinlove, G. Worth, I. Burghardt, and B. Lasorne, *Int. Rev. Phys. Chem.* **34**, 269 (2015).
- ³¹M. Wehrle, M. Šulc, and J. Vaníček, *J. Chem. Phys.* **140**, 244114 (2014).
- ³²M. Wehrle, S. Oberli, and J. Vaníček, *J. Phys. Chem. A* **119**, 5685 (2015).
- ³³A. Lami, C. Petrongolo, and F. Santoro, in *Conical intersections: Electronic structure, dynamics and spectroscopy*, edited by W. Domcke, D. R. Yarkony, and H. Köppel (World Scientific Publishing, Singapore, 2004) Chap. 16, pp. 699–738.
- ³⁴Y. Niu, Q. Peng, C. Deng, X. Gao, and Z. Shuai, *J. Phys. Chem. A* **114**, 7817 (2010).
- ³⁵M. A. Rohrdanz and J. A. Cina, *Mol. Phys.* **104**, 1161 (2006).

- ³⁶T. Begušić, J. Roulet, and J. Vaníček, *J. Chem. Phys.* **149**, 244115 (2018).
- ³⁷M. Ceotto, Y. Zhuang, and W. L. Hase, *J. Chem. Phys.* **138**, 054116 (2013).
- ³⁸Y. Zhuang, M. R. Siebert, W. L. Hase, K. G. Kay, and M. Ceotto, *J. Chem. Theory Comput.* **9**, 54 (2013).
- ³⁹R. Ianculescu, J. Tatchen, and E. Pollak, *J. Chem. Phys.* **139**, 154311 (2013).
- ⁴⁰J. P. Alborzpour, D. P. Tew, and S. Habershon, *J. Chem. Phys.* **145**, 174112 (2016).
- ⁴¹G. Laude, D. Calderini, D. P. Tew, and J. O. Richardson, *Faraday Discuss.* (2018), 10.1039/C8FD00085A.
- ⁴²G. Di Liberto and M. Ceotto, *J. Chem. Phys.* **145**, 144107 (2016).
- ⁴³J. Tatchen, E. Pollak, G. Tao, and W. H. Miller, *J. Chem. Phys.* **134** (2011), 10.1063/1.3573566.
- ⁴⁴F. J. Avila Ferrer and F. Santoro, *Phys. Chem. Chem. Phys.* **14**, 13549 (2012).
- ⁴⁵A. Patoz, T. Begušić, and J. Vaníček, *J. Phys. Chem. Lett.* **9**, 2367 (2018).
- ⁴⁶T. Begušić, A. Patoz, M. Šulc, and J. Vaníček, *Chem. Phys.* **515**, 152 (2018).
- ⁴⁷J. Cerezo, J. Zuniga, A. Requena, F. J. Ávila Ferrer, and F. Santoro, *J. Chem. Theory Comput.* **9**, 4947 (2013).
- ⁴⁸E. J. Heller, *J. Chem. Phys.* **75**, 2923 (1981).
- ⁴⁹H.-J. Werner, P. J. Knowles, G. Knizia, F. R. Manby, and M. Schütz, *WIREs Comput. Mol. Sci.* **2**, 242 (2012).
- ⁵⁰H.-J. Werner, P. J. Knowles, G. Knizia, F. R. Manby, M. Schütz, P. Celani, T. Korona, R. Lindh, A. Mitrushenkov, G. Rauhut, K. R. Shamasundar, T. B. Adler, R. D. Amos, A. Bernhardsson, A. Berning, D. L. Cooper, M. J. O. Deegan, A. J. Dobbyn, F. Eckert, E. Goll, C. Hampel, A. Hesselmann, G. Hetzer, T. Hrenar, G. Jansen, C. Köppl, Y. Liu, A. W. Lloyd, R. A. Mata, A. J. May, S. J. McNicholas, W. Meyer, M. E. Mura, A. Nicklass, D. P. O’Neill, P. Palmieri, D. Peng, K. Pflüger, R. Pitzer, M. Reiher, T. Shiozaki, H. Stoll, A. J. Stone, R. Tarroni, T. Thorsteinsson, and M. Wang, “Molpro, version 2012.1, a package of ab initio programs,” (2012), see <http://www.molpro.net>.
- ⁵¹M. J. Frisch, G. W. Trucks, H. B. Schlegel, G. E. Scuseria, M. A. Robb, J. R. Cheeseman, G. Scalmani, V. Barone, B. Mennucci, G. A. Petersson, H. Nakatsuji, M. Caricato, X. Li, H. P. Hratchian, A. F. Izmaylov, J. Bloino, G. Zheng, J. L. Sonnenberg, M. Hada, M. Ehara, K. Toyota, R. Fukuda, J. Hasegawa, M. Ishida, T. Nakajima, Y. Honda, O. Kitao, H. Nakai, T. Vreven, J. A. Montgomery, Jr., J. E. Peralta, F. Ogliaro, M. Bearpark,

- J. J. Heyd, E. Brothers, K. N. Kudin, V. N. Staroverov, R. Kobayashi, J. Normand, K. Raghavachari, A. Rendell, J. C. Burant, S. S. Iyengar, J. Tomasi, M. Cossi, N. Rega, J. M. Millam, M. Klene, J. E. Knox, J. B. Cross, V. Bakken, C. Adamo, J. Jaramillo, R. Gomperts, R. E. Stratmann, O. Yazyev, A. J. Austin, R. Cammi, C. Pomelli, J. W. Ochterski, R. L. Martin, K. Morokuma, V. G. Zakrzewski, G. A. Voth, P. Salvador, J. J. Dannenberg, S. Dapprich, A. D. Daniels, O. Farkas, J. B. Foresman, J. V. Ortiz, J. Cioslowski, and D. J. Fox, "Gaussian 09 Revision D.01," Gaussian Inc. Wallingford CT 2009.
- ⁵²S. L. Tang, D. G. Imre, and D. Tannor, *J. Chem. Phys.* **92**, 5919 (1990).
- ⁵³S. L. Tang, E. H. Abramson, and D. G. Imre, *J. Phys. Chem.* **95**, 4969 (1991).
- ⁵⁴A. Capobianco, R. Borrelli, C. Noce, and A. Peluso, *Theor. Chem. Acc.* **131**, 1 (2012).
- ⁵⁵A. Baiardi, J. Bloino, and V. Barone, *J. Chem. Theory Comput.* **13**, 2804 (2017).
- ⁵⁶F. Chen, D. Judge, C. Wu, and J. Caldwell, *Planet. Space Sci.* **47**, 261 (1999).
- ⁵⁷R. S. Becker, J. S. D. de Melo, L. A. Macanita, and F. Elisei, *J. Phys. Chem.* **100**, 18683 (1996).